Journal of Zhejiang University-SCIENCE A (Applied Physics & Engineering) 2025 26(4):376-388
www.jzus.zju.edu.cn; www.springer.com/journal/11582
E-mail: jzus_a@zju.edu.cn

Research Article

https://doi.org/10.1631/jzus.A2400252

Prediction of wheel wear in light rail trains using an improved grey GM(1,1) model

Yanyan ZHANG[1], Xinwen YANG[1]✉, Zhiang SUN[1], Kaiwen XIANG[1], Anguo ZUO[2]

[1]*Shanghai Key Laboratory of Rail Infrastructure Durability and System Safety, Tongji University, Shanghai 201804, China*
[2]*Operation Business Department, Changchun Railway Traffic Group Co., Ltd., Changchun 130012, China*

Abstract: The wheel wear of light rail trains is difficult to predict due to poor information and small data samples. However, the amount of wear gradually increases with the running mileage. The grey future prediction model is supposed to deal with this problem effectively. In this study, we propose an improved non-equidistant grey model GM(1,1) with background values optimized by a genetic algorithm (GA). While the grey model is not good enough to track data series with features of randomness and nonlinearity, the residual error series of the GA-GM(1,1) model is corrected through a back propagation neural network (BPNN). To further improve the performance of the GA-GM(1,1)-BPNN model, a particle swarm optimization (PSO) algorithm is implemented to train the weight and bias in the neural network. The traditional non-equidistant GM(1,1) model and the proposed GA-GM(1,1), GA-GM(1,1)-BPNN, and GA-GM(1,1)-PSO-BPNN models were used to predict the wheel diameter and wheel flange wear of the Changchun light rail train and their validity and rationality were verified. Benefitting from the optimization effects of the GA, neural network, and PSO algorithm, the performance ranking of the four methods from highest to lowest was GA-GM(1,1)-PSO-BPNN>GA-GM(1,1)-BPNN>GA-GM(1,1)>GM(1,1) in both the fitting and prediction zones. The GA-GM(1,1)-PSO-BPNN model performed best, with the lowest fitting and forecasting maximum relative error, mean absolute error, mean absolute percentage error, and mean squared error of all four models. Therefore, it is the most effective and stable model in field application of light rail train wheel wear prediction.

Key words: Wheel wear prediction; Grey model; Genetic algorithm (GA); Neural network; Particle swarm optimization (PSO)

1 Introduction

C-type 6-module low-floor trains are operated on the Changchun light rail lines in China (Liu et al., 2022). The train has only one bogie located under each car body and the car bodies are articulated with each other by joints, which introduce an extra rotational degree of freedom on the car body. This causes excessive bending between car bodies and consequently aggravates the wheel wear problem. According to the statistics of wheel–rail wear of Changchun light rail lines from 2019 to now, significant abnormal wheelset flange wear and tread wear exceeding maintenance standards are commonly found, leading to the degeneration of train operational safety, passenger riding comfort, and wheel and rail service life. It follows that making more accurate predictions of wheel wear in the future is crucial to providing a reference for timely wheel reprofiling or replacement so as to reduce vehicle operation costs and ensure operation quality.

Many methods aiming to predict wheel wear have been developed in recent decades. The model-driven method combines the vehicle–track coupled dynamics model and the material wear model to numerically simulate and predict wheel–rail contact wear. The key point in the model-driven method is to solve the vehicle–rail dynamics problem and the wheel–rail rolling contact problem. Typical material wear models include those based on the Archard model (Chudzikiewicz and Korzeb, 2018; Wang et al., 2022b), friction work model (Correa et al., 2016; Wojciechowski et al., 2020), and wear index model (Jiang et al., 2019). Of these models, the Archard model is the most commonly used. According to the Archard model, the material wear of

✉ Xinwen YANG, xinwenyang@tongji.edu.cn
Yanyan ZHANG, https://orcid.org/0000-0002-5896-4123
Xinwen YANG, https://orcid.org/0000-0001-8209-1257

Received May 14, 2024; Revision accepted June 20, 2024;
Crosschecked Mar. 13, 2025

the wheel is directly proportional to the wheel–rail normal contact force and relative sliding distance, and inversely proportional to the hardness of the worn material (Pradhan et al., 2019). However, the wheel flange wear prediction results based on the Archard model are inferior to those of the other two models, while the wheel diameter prediction effects of the three models are equivalent (Zhu Y et al., 2019).

Before using a material wear model, it is necessary to develop physical models of the vehicle and track to obtain the vehicle dynamics characteristics and wheel–rail contact characteristics. The finite element method is feasible but complex (Łuczak et al., 2020). The calculation accuracy and the expense of the computational effort are often in conflict and need to be balanced. However, finite element method can provide convincing results. Popular commercial software such as UM (Wang et al., 2022b) and SIMPACK (Zhu AH et al., 2019; Wang SW et al., 2022) contain a wheel–rail wear simulation module which integrates a vehicle dynamics model, wheel–rail contact model, and material wear model. By using the easy-to-use software, the dynamic responses of the physical model can be calculated and the wheel and rail wear can be predicted efficiently and rapidly.

With increasing operating mileage, a massive amount of historical tracking wheel wear data has been accumulated. This enables deep analysis of the useful information in these long-term datasets and so a number of data-driven wheel wear prediction methods have emerged. Generally, data-driven methods contain two types of models: a probability statistical model and a machine learning method. The statistical model focuses on fitting a linear or nonlinear relationship between wheel wear and time or mileage by methods such as the least squares method (Han and Zhang, 2015; Zhu AH et al., 2019), grey model (Li et al., 2015), Markov decision process model (Jiang et al., 2017), Monte Carlo model (Yang et al., 2018), and Bayesian data-driven model (Chi et al., 2020).

Under the sustainable development of intelligent and information technology, machine learning has been the ideal choice to deal with large-scale datasets. Machine learning extracts the features from the given data, finds the knowledge and rule in the data, builds the mathematical model for the data, self-corrects the mathematical model over time, and then forecasts future data. The most well-known machine learning for wheel wear prediction is artificial neural network technology, including conventional neural network (Wang SW et al., 2022), non-linear autoregressive neural network (NARNN) (Fan et al., 2017), nonlinear autoregressive model with exogenous input neural network (NARXNN) (Shebani and Iwnicki, 2018), Levenberg Marquardt back propagation neural network (LMBPNN) (Zhang et al., 2019), and Levenberg Marquardt (LM)-orthogonal matching pursuit (OMP)-NARXNN model (Deng et al., 2023). Neural network models can easily become trapped into local extreme values and so the weight and bias in the network usually need to be optimized through several non-numerical optimization algorithms, such as ant colony algorithm (Chang et al., 2022), particle swarm optimization (PSO) algorithm (Cai H et al., 2022), genetic algorithm (GA) (Su et al., 2023), or simulated annealing (SA) algorithm (Yuan et al., 2024).

Support vector machine (SVM)/support vector regression (SVR) and extreme learning machine (ELM) are two other developed machine learning models for wheel wear forecasting. Similar to the conventional neural network, traditional SVM/SVR might also be inclined to seek out the local optimal value. In this case, grey wolf optimizer (GWO) optimized multi-core SVR (Xu, 2021), GA-SVR (Liao, 2014), PSO-SVR (Xing et al., 2014), and coupled SA optimized least squares SVM (Zhong et al., 2015) are optional to replace the traditional SVM/SVR. ELM was proposed based on a single hidden layer feedforward neural network and has the advantages of a faster training speed and higher training accuracy (Huang et al., 2006). However, the improved ELM models, e.g., PSO optimized multi-kernel ELM (Chen, 2019), multilayer ELM with identity mapping (Wang et al., 2022a), and chaotic quantum PSO optimized derived ELM (Wang et al., 2022b), are undoubtedly more attractive and successful. In summary, although the data-driven method avoids the need for an in-depth understanding of detailed and complex physical processes, it still depends heavily on the quantity and quality of the observed data. For small samples with deficient information, a data-driven method is not sufficiently accurate.

Wheel wear becomes more serious with increasing running mileage. Generally, the detected wear forms a small non-equidistant sample. Grey system theory is particularly suitable for processing this kind of dataset. In the present study, the non-equidistant GM(1,1) model

was used to predict the growth of wheel wear in light rail trains on the Changchun light rail line. The background value of the traditional GM(1,1) model is approximately constructed using a trapezoidal area formula, which causes a large error when the sample interval is large or the accumulating series increases sharply (Cai L et al., 2022). The dynamic adaptive factor varying with the observed mileage interval was introduced by Li et al. (2016) to the traditional background value calculation formula to achieve a background value closer to the theoretical value. However, there is no universal principle for the appropriate selection of these dynamic adaptive factors. Hence, in this work, we implemented GA to seek rational dynamic adaptive factors to improve the performance of the traditional grey model. The grey theory can predict how the wheel wear will deteriorate in the future but cannot capture the random section and periodic section in the original dataset. Conversely, neural network technology is particularly strong in analyzing nonlinear samples (Zhang et al., 2016). In view of this, the GA-GM(1,1) model was further improved by correcting its initial residual errors using a back propagation neural network (BPNN) model. The optimal weights and biases of the network are automatically searched by a PSO algorithm. The fitting and prediction accuracies of the traditional GM(1,1) model and the three improved models proposed in this paper, i.e., GA-GM(1,1), GA-GM(1,1)-BPNN, and GA-GM(1,1)-PSO-BPNN, were estimated by the maximum relative error (MRE), mean absolute error (MAE), mean absolute percentage error (MAPE), and mean squared error (MSE). The effectiveness and stability of the four models were compared and analyzed quantitatively.

2 GA-GM(1,1) model

2.1 Traditional non-equidistant GM(1,1) model

The non-equidistant series is converted to an equidistant series with the help of the unit time difference factor and then the GM(1,1) model is established making use of the obtained equidistant series. Let $X^{(0)}(s)=\{x^{(0)}(s_1), x^{(0)}(s_2), \cdots, x^{(0)}(s_n)\}$ be a non-equidistant mileage wheel wear measurement series with the measured running mileage interval $\Delta s_i=s_i-s_{i-1}\neq$const, i=2, 3, $\cdots$, n. The average measured mileage interval is:

$$\Delta s_0=\frac{s_n-s_1}{n-1}. \tag{1}$$

The unit time difference factor between each measured mileage interval and the average measured mileage interval is:

$$\mu(s_i)=\frac{s_i-s_1-(i-1)\Delta s_0}{\Delta s_0}. \tag{2}$$

The total difference in each measured period is:

$$\Delta x^{(0)}(s_i)=\mu(s_i)[x^{(0)}(s_i)-x^{(0)}(s_{i-1})]. \tag{3}$$

The grey values at equal interval are calculated as follows:

$$z^{(0)}(s_i)=x^{(0)}(s_i)-\Delta x^{(0)}(s_i). \tag{4}$$

Then, the reconstructed evenly spaced data series can be represented as $Z^{(0)}(s)=\{z^{(0)}(s_1), z^{(0)}(s_2), \cdots, z^{(0)}(s_n)\}$. Based on this, the first-order accumulative generating operator (1-AGO) series of $Z^{(0)}(s)$ is $Z^{(1)}(s)=\{z^{(1)}(s_1), z^{(1)}(s_2), \cdots, z^{(1)}(s_n)\}$.

A GM(1,1) model is established for $Z^{(1)}(s)$, the whitening differential equation is:

$$\frac{\mathrm{d}z^{(1)}}{\mathrm{d}s}+az^{(1)}=b, \tag{5}$$

where a and b are the parameters to be estimated by the least squares method. Their estimated values are:

$$[a,\ b]^{\mathrm{T}}=(\boldsymbol{B}^{\mathrm{T}}\boldsymbol{B})^{-1}\boldsymbol{B}^{\mathrm{T}}\boldsymbol{Y}, \tag{6}$$

where $\boldsymbol{B}$ and $\boldsymbol{Y}$ are defined as follows:

$$\boldsymbol{B}=\begin{bmatrix}-\bar{z}^{(1)}(s_2) & 1\\ -\bar{z}^{(1)}(s_3) & 1\\ \vdots & \vdots\\ -\bar{z}^{(1)}(s_n) & 1\end{bmatrix},\quad \boldsymbol{Y}=\begin{bmatrix}z^{(0)}(s_2)\\ z^{(0)}(s_3)\\ \vdots\\ z^{(0)}(s_n)\end{bmatrix}, \tag{7}$$

with

$$\bar{z}^{(1)}(s_i)=\frac{z^{(1)}(s_i)+z^{(1)}(s_{i-1})}{2}. \tag{8}$$

Solving Eq. (5), the time response function of the whitening differential equation is:

$$\hat{z}^{(1)}(s_i)=\left[z^{(0)}(s_1)-\frac{b}{a}\right]\mathrm{e}^{-a(s_i-1)}+\frac{b}{a},\ i=1,\ 2,\ \cdots,\ n. \quad (9)$$

Let $\hat{x}^{(0)}(s_1)=x^{(0)}(s_1)$, the predicted values of the original measured wheel wear series are as follows:

$$\hat{x}^{(0)}(s_i)=(1-\mathrm{e}^{a})\left[x^{(0)}(s_1)-\frac{b}{a}\right]\mathrm{e}^{-\frac{a(s_i-s_1)}{\Delta s_0}},\ i=2,\ 3,\ \cdots,\ n. \quad (10)$$

2.2 GA optimized background value

$\bar{z}^{(1)}(s_i)$ is called the background value series of the GM(1,1) model. It is one of the sources of error in parameter estimation by the grey model. The theoretical background value is the area enclosed by the curve of the nonlinear function $Z^{(1)}(s)$ on $[s_{i-1}, s_i]$ and s-axis, which is expressed as $\int_{s_{i-1}}^{s_i} Z^{(1)}(s)\mathrm{d}s$. According to Eq. (8), the background value is taken as the average value of the two points $z^{(1)}(s_i)$ and $z^{(1)}(s_{i-1})$. That is, the background value is the area of the trapezoid $ABCD$ (Fig. 1). There is an apparent error between the two background value calculation methods which becomes unacceptable when the sample interval is large and the 1-AGO series grows sharply.

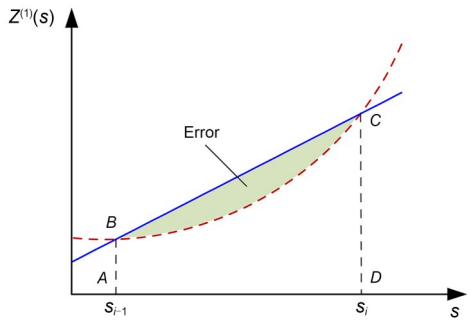

Fig. 1 Background value construction of the GM(1,1) model

In Eq. (8), the weights of $z^{(1)}(s_i)$ and $z^{(1)}(s_{i-1})$ are equal (=0.5), which does not agree with the adjacent two measurement intervals probably being different.

To consider the effect of the measurement interval, a dynamic adaptive factor varying with the observed mileage interval was introduced by Li et al. (2016) to revise Eq. (8) as follows:

$$\bar{z}^{(1)}(s_i)=\lambda_i z^{(1)}(s_i)+(1-\lambda_i)z^{(1)}(s_{i-1}), \quad (11)$$

where λ_i ($0\leqslant\lambda_i\leqslant1$) is the dynamic adaptive factor.

However, how to properly determine the value of the dynamic adaptive factor is a puzzling problem. We can do this job using an intelligent algorithm. A GA traverses the whole search space and searches for several local optimal solutions, thus increasing the possibility of finding a global optimal solution. With the minimum prediction error of GM(1,1) as the constraint condition, in this study, we regarded the dynamic adaptive factors as variables and searched for the optimal solutions by GA. The steps were as follows:

Step 1: Encoding and population initialization. Chromosomes are encoded by real numbers and a single chromosome can be treated as a string of real numbers. Each chromosome includes all the adaptive factors of the background value series as $\{\lambda_2, \lambda_3, \cdots, \lambda_n\}$. Hence, the encoding length is $n-1$. n_g initial chromosomes are randomly generated within a preset gene assignment range, where n_g is the population size. Each chromosome in the population corresponds to one individual.

Step 2: Population fitness evaluation. The adaptive factors carried by each individual are assigned to the corresponding background values. The wheel wear is forecasted by the GM(1,1) model. We design the fitness function in the same direction as the prediction error optimization. The smaller the fitness, the better the individual. Therefore, a forecast accuracy evaluation indicator is selected as the individual fitness function.

Step 3: Selection operation. The roulette selection strategy is adopted to choose better individuals in the population. Supposing the fitness value of individual i is F_i, all the individuals are sorted from largest to smallest according to their fitness. The probability p_i of each individual being selected is calculated as follows:

$$p_i=\frac{F_i}{\sum_{j=1}^{n_g}F_j}. \quad (12)$$

The range [0, 1] is divided into n_g intervals according to the selection probabilities. Generating a random number between 0 and 1, the individual with p_i corresponding to the interval within which the random number falls will be picked out.

Step 4: Crossover operation. Based on a preset crossover probability P_c, two individuals denoted the

*i*th and *j*th chromosomes are randomly selected from the population and are cut at the same location, position *k*. The gene segments of the selected individuals between position *k* and the terminal position are exchanged, as shown in Eq. (13)(Ning et al., 2022):

$$\begin{cases} a_{ikt}=b_{\mathrm{r}}a_{jkt}+(1-b_{\mathrm{r}})\,a_{ikt}, \\ a_{jkt}=b_{\mathrm{r}}a_{ikt}+(1-b_{\mathrm{r}})\,a_{jkt}, \end{cases} \tag{13}$$

where a_{ikt} and a_{jkt} are the gene segments of the *i*th and *j*th chromosomes between position *k* and the terminal position, respectively; b_{r} is a random number and $b_{\mathrm{r}}\in[0, 1]$.

Step 5: Mutation operation. Based on a preset mutation probability P_{m}, the *i*th chromosome is selected from the population to enter the mutation phase. The *k* gene of this individual is changed, as shown in Eq. (14) (Liu et al., 2024):

$$a_{ik}=\begin{cases} a_{ik}+(a_{ik}-a_{ik\max})\cdot f(g), & r_1\geqslant 0.5, \\ a_{ik}+(a_{ik\min}-a_{ik})\cdot f(g), & r_1<0.5, \end{cases} \tag{14}$$

with

$$f(g)=r_2\left(1-\frac{g}{g_{\max}}\right)^2, \tag{15}$$

where a_{ik} is the gene of the *i*th chromosome at *k* position; $a_{ik\max}$ and $a_{ik\min}$ are the upper and lower bounds of the selected gene, respectively; r_1 and r_2 are two random numbers, $r_1\in[0, 1]$ and $r_2\in[0, 1]$; g is the current evolution number; $g_{\max}$ is the maximum evolution number.

Step 6: Ending condition. The new population is created after the selection, crossover, and mutation operations. The fitness of each offspring individual is calculated and the optimal individual is the one with the minimum fitness. Steps 3 to 5 are repeated and the set of initial dynamic adaptive factors evolves continuously until the fitness of the optimal chromosome is less than the desired one or the evolution number has reached the preset value.

The combination of dynamic adaptive factors corresponding to the optimal individual is then delivered to Eq. (11) to modify the background value series in the traditional non-equidistant GM(1,1) model.

3 BPNN residual error correction model

3.1 BPNN architecture

BPNN is a typical multi-layer feedforward neural network. Its basic structure includes an input layer, a hidden layer, and an output layer. The most typical BPNN is a three-layer network which has a single hidden layer (Fig. 2a) because it can realize the mapping between input and output with arbitrary dimensions. The input and output data are two *m*- and *n*-dimensional vectors: $\boldsymbol{X}=(x_1, x_2, \cdots, x_m)^{\mathrm{T}}\in\mathbb{R}^m$ and $\boldsymbol{Y}=(y_1, y_2, \cdots, y_n)^{\mathrm{T}}\in\mathbb{R}^n$ while the hidden layer has *p* nodes represented by h_1 to h_p. The input data flow is uniquely directed from the first layer to the last layer through interconnected nodes. The nodes, called neurons, in the same layer are not connected to each other, but are connected to all nodes in the adjacent layer. Each neuron, composed of a summation operator and an activation function *f*, receives input signals from all the neurons in upper layers and produces an output after applying the activation function to the weighted sum of its inputs. The output information of a neuron is given by:

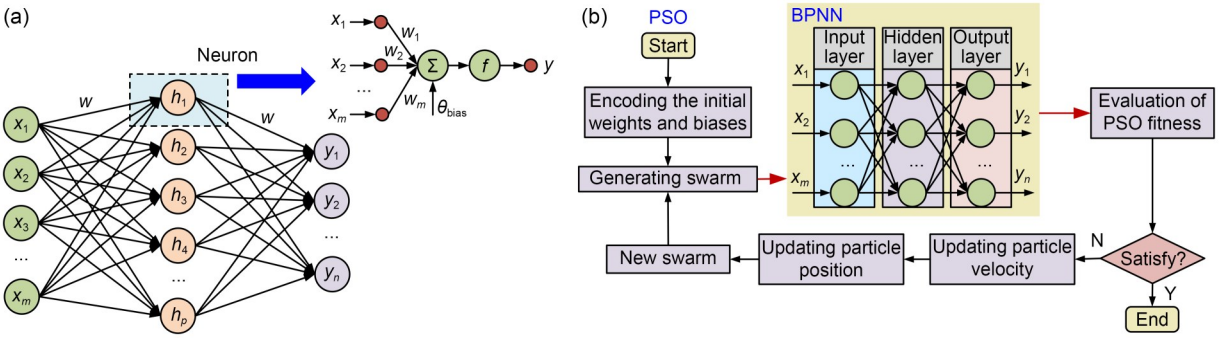

Fig. 2 Topology of standard BPNN (a) and PSO-BPNN (b)

$$y=f\left(\sum_{i=1}^{m}w_i x_i+\theta_{\text{bias}}\right), \tag{16}$$

where $w_i\in\mathbb{R}$ is the ith connection weight; x_i is the ith input signal; $\theta_{\text{bias}}\in\mathbb{R}$ is the bias factor.

Initially, all the weights and biases are assigned values randomly. During network training, the network compares the actual output with the desired output and propagates the total error through a backpropagation algorithm to each node in every layer. As a result, the weight and bias parameters are adjusted dynamically to minimize the performance function.

3.2 PSO optimized BPNN

PSO is a biology-inspired evolutionary computation algorithm originating from the social behavior of predatory birds. It has the advantages of an easy update mechanism, fewer parameters, quick convergence, and global search performance. The PSO starts with a swarm, which is a gathering of arbitrary particles characterized by irregular positions and velocities. Each particle travels its position toward the best position through hyperspace scanning based on its, and the swarm's, previous experience. In the progression, the new location of a particle is updated by adding a velocity to its existing position. The updating processes of particle velocity and position are as follows:

$$x_i^{k+1}=x_i^k+v_i^{k+1}, \tag{17}$$

$$v_i^{k+1}=wv_i^k+c_1r_1(p_{\text{best}}^k-x_i^k)+c_2r_2(g_{\text{best}}^k-x_i^k), \tag{18}$$

where x_i^{k+1} and x_i^k are the positions of the ith particle in the (k+1)th and kth iterations, respectively; v_i^{k+1} and v_i^k are the velocities of the ith particle in the (k+1)th and kth iterations, respectively; w is the inertia weight and $w\in[0, 1.2]$; c_1 and c_2 are acceleration constants within the interval of [0, 2]; r_1 and r_2 are random numbers within the interval of [0, 1]; p_{best}^k and g_{best}^k are the best individual and global positions, respectively, of particles in the kth iteration.

The traditional BPNN model has a sluggish convergence rate and is easily trapped into a local extreme value. Also, BPNN is sensitive to the initial connection weights and biases. For this reason, the PSO algorithm is used to optimize the network weight and bias parameters to reduce the weaknesses of BPNN. The topology of PSO-BPNN is shown in Fig. 2b. The steps of weight and bias optimization are as follows:

Step 1: Encoding and swarm initialization. Similar to GA, a real-number encoding style is used for a particle containing all the weights and biases of a BPNN. Each particle can be expressed according to the topology of the neural network as $\{w_{11}^2, w_{21}^2, \cdots, w_{np}^3, \theta_{\text{bias1}}^2, \theta_{\text{bias2}}^2, \cdots, \theta_{\text{biasn}}^3\}$, where the superscripts 2 and 3 denote the hidden and output layers, respectively, w_{ij} is the weight between the ith neuron and the jth neuron in the upper layer, and $\theta_{\text{bias}i}$ is the ith bias. Subsequently, the encoding length is given by:

$$L=(m+n+1)\,p+n. \tag{19}$$

Limiting the position and velocity assignment ranges, n_{p} initial particles are randomly generated, where n_{p} is the population size of the swarm.

Step 2: Fitness evaluation. The weights and biases in each particle are assigned to the corresponding positions in the BPNN. The network is then trained and the test samples are predicted. A forecast accuracy evaluation indicator is taken as the particle fitness function. The fitness value of each particle is calculated and the optimal individual and global fitness (the minimum forecast error) are chosen.

Step 3: Updating the velocity and position of each particle. Using Eqs. (17) and (18), the new swarm is generated.

Step 4: Ending condition. The weight and bias optimization process will be terminated when the global fitness is less than expected or the evolution number has reached the preset value. The weights and biases corresponding to the optimal individual are then delivered to the BPNN model. The network continues to be trained until the learning goal is met or the training epoch reaches the preset target. Otherwise, go to Step 3 to conduct a new cycle of velocity and position updating on the evolved population.

3.3 GA-GM(1,1)-PSO-BPNN model

The wheel wear of a light rail train is affected in variable degrees by many factors such as the line condition, running speed, tread profile, and contact geometry. As a result, the changing trend of wheel wear is nonlinear and random. Moreover, there are occasional errors in the measured wear data. Faced with these circumstances, a grey model can do little. Unlike the GM(1,1) model, neural network technology is particularly strong in analyzing nonlinear samples. It can fully

learn the mutation data during the training process and eliminate the interference of random factors. Therefore, the grey model and the neural network can be integrated to produce a quantitative and qualitative forecasting method. Correcting the initial residual errors of the GM(1,1) model by BPNN is one of the main methods to improve the grey prediction performance. The specific principle of the GA-GM(1,1)-PSO-BPNN model for wheel wear prediction is shown in Fig. 3.

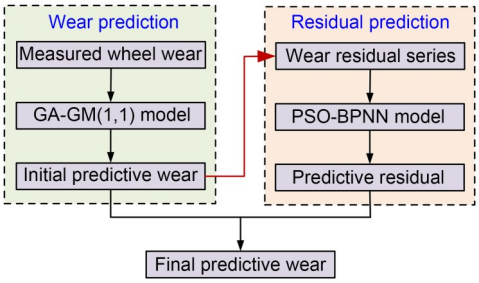

Fig. 3 Flow chart of the GA-GM(1,1)-PSO-BPNN model for wheel wear prediction

Step 1: The GA-GM(1,1) model is used to analyze and forecast the measured wheel wear dataset, and the initial predicted series of wear is obtained: $\hat{X}^{(0)}(s)=\{\hat{x}^{(0)}(s_1), \hat{x}^{(0)}(s_2), \cdots, \hat{x}^{(0)}(s_n)\}$.

Step 2: The residual error series between the initial predicted wear series and the measured wear series is calculated according to the following equation:

$$E^{(0)}(s)=X^{(0)}(s)-\hat{X}^{(0)}(s). \tag{20}$$

Step 3: The residual error series is taken as the input of the PSO-BPNN model. The PSO-BPNN model is then trained and the predictive residual error series $\hat{E}^{(0)}(s)=\{\hat{e}^{(0)}(s_1), \hat{e}^{(0)}(s_2), \cdots, \hat{e}^{(0)}(s_n)\}$ is output.

Step 4: The initial predictive wear of the GA-GM(1,1) model is corrected by the predictive residual error values of the PSO-BPNN model to obtain the final predictive wear series $\hat{X}^{(0)}_{\text{pre}}(s)=\{\hat{x}^{(0)}_{\text{pre}}(s_1), \hat{x}^{(0)}_{\text{pre}}(s_2), \cdots, \hat{x}^{(0)}_{\text{pre}}(s_n)\}$, as shown in Eq. (21).

$$\hat{X}^{(0)}_{\text{pre}}(s)=\hat{X}^{(0)}(s)+\hat{E}^{(0)}(s). \tag{21}$$

The relative error (RE), MAE, MAPE, and MSE between the final predictive wear series and the measured one are chosen as the forecast accuracy evaluation indicators. The formulas of RE (E_{R}), MAE (E_{MA}), MAPE (E_{MAP}), and MSE (E_{MS}) are as follows:

$$E_{\text{R}i}=\frac{x^{(0)}(s_i)-\hat{x}^{(0)}_{\text{pre}}(s_i)}{x^{(0)}(s_i)}\times 100\%,\quad i=1, 2, \cdots, n, \tag{22}$$

$$E_{\text{MA}}=\frac{1}{n}\sum_{i=1}^{n}|\hat{x}^{(0)}_{\text{pre}}(s_i)-x^{(0)}(s_i)|, \tag{23}$$

$$E_{\text{MAP}}=\frac{1}{n}\sum_{i=1}^{n}\left|\frac{\hat{x}^{(0)}_{\text{pre}}(s_i)-x^{(0)}(s_i)}{x^{(0)}(s_i)}\right|\times 100\%, \tag{24}$$

$$E_{\text{MS}}=\frac{1}{n}\sum_{i=1}^{n}[\hat{x}^{(0)}_{\text{pre}}(s_i)-x^{(0)}(s_i)]^2. \tag{25}$$

4 Wheel wear prediction of light rail train

4.1 Field test

The Changchun Rail Transit Line 4 starts from the Changchun Railway Station (North) and ends at the Tianxin Road Station. It is 20.82 km long and serves as a medium-volume auxiliary line in the light rail network. The trains operated on this line are in the form of −Mc1+Tp1+M1−M2+Tp2+Mc2−, where Mc and M represent the motor vehicles with and without cabs, respectively, Tp represents the trailer vehicle with a pantograph, "−" represents the semi-permanent coupler, and "+" represents the single articulated device. Their maximum operating speed is 70 km/h. We monitored the wheel wear of all the wheelsets for months on these trains (Fig. 4). Statistical analysis showed that the wheel wear was concentrated mainly near the flange and tread root, so two parameters, wheel diameter and wheel flange wear, were considered for prediction in this study. The 17 sets of wheel diameter and flange wear data of the guiding wheel in the Mc1 module of a light rail train were taken to verify the applicability of the three prediction models proposed above. The mileage sampling intervals of the sequences obtained differed. The inspection data are shown in Table 1.

Fig. 4 Wheel wear photographs from a light rail train

4.2 Variable selection

The inspection data were divided into 12, 13, and 14 dimensions to develop six groups of non-equidistant

Table 1 Measured data of wheel diameter and wheel flange wear

No.	Mileage (km)	Wheel diameter (mm)	Wheel flange wear (mm)
1	465523	660.0	1.2456
2	496271	659.6	1.3730
3	525525	658.1	1.5002
4	557825	657.5	1.6544
5	580318	654.5	1.8368
6	609647	654.1	2.0072
7	645822	653.8	2.2434
8	679827	653.7	2.5814
9	708954	653.5	2.7396
10	736453	653.3	2.8441
11	767652	651.8	2.8053
12	798292	651.4	2.9071
13	832159	651.1	3.0220
14	865527	650.5	3.2365
15	894857	649.9	3.2205
16	928513	649.6	3.5798
17	959875	648.8	3.7181

GM(1,1) models. For example, the i-dimensional model predicts the subsequent $n-i$ data based on the first i samples. The prediction results of the 12-, 13-, and 14-dimensional models are shown in Table 2. Model performance was closely related to the data dimension and the prediction step. Because the prediction error accumulates with the increase of the prediction step, the accuracy of the 13- and 14-dimensional models was higher than that of the 12-dimensional model. Thus, the 14-dimensional GM(1,1) model, i.e. 14 sets of training samples, was used in the following forecast of wheel wear.

In modeling GA, the gene assignment range was set as [0, 1] and the individual fitness function was MAPE. The other preset parameters were as follows: population size, 50; maximum evolution number, 100; crossover probability, 0.8; mutation probability, 0.2; evolution goal of individual fitness, 1×10^{-6}.

During residual error prediction using BPNN, multi-step scroll prediction was used to ensure prediction accuracy because of the small data samples. i consecutive sets of samples were taken as the input, and the (i+1)th sample was taken as the expected output. The numbers of neurons in input, hidden, and output layers were determined through trial-and-error methods as 5, 6, and 1, respectively, for the wheel diameter prediction model and 3, 10, and 1 for the wheel flange wear model. The activation function used in this study was "tansig" (Eq. (26)). The input to this function can be an arbitrary value and its output is within [−1, 1], so the inputs of each layer are unified.

$$\tan\mathrm{sig}(x)=\frac{2}{1+\mathrm{e}^{-2x}}-1. \tag{26}$$

The other preset parameters were as follows: maximum training epoch, 1000; learning goal, 1×10^{-6}; learning rate, 0.001; minimum performance gradient, 1×10^{-6}; additional momentum factor, 0.95; the performance function used in training was the MSE.

In modeling the PSO algorithm, the position and velocity assignment ranges were both set as [−3, 3] to ensure a large search space. The MAPE was taken as the particle fitness function. The other preset parameters were as follows: population size, 100; maximum iteration number, 100; inertia weight, 0.9; the two acceleration constants were both 0.6; the evolution goal of individual fitness was 1×10^{-6}.

Table 2 Prediction results of the 12-, 13-, and 14-dimensional models

No.	Wheel diameter (mm)				Wheel flange wear (mm)			
	Actual	12-dimensional	13-dimensional	14-dimensional	Actual	12-dimensional	13-dimensional	14-dimensional
13	651.1	650.2			3.022	3.376		
14	650.5	649.4	649.7		3.237	3.653	3.483	
15	649.9	648.7	649.1	649.3	3.221	3.916	3.712	3.609
16	649.6	647.9	648.3	648.6	3.580	4.242	3.993	3.868
17	648.8	647.2	647.6	647.9	3.718	4.569	4.273	4.125
MRE (%)		0.26	0.20	0.16		22.88	15.26	12.07
MAE (mm)		1.294	1.020	0.841		0.596	0.427	0.361
MAPE		0.002	0.002	0.001		0.175	0.123	0.104
MSE (mm^2)		1.767	1.090	0.740		0.389	0.195	0.133

4.3 Empirical results

A comparison of the error convergence trends of the training processes between the proposed GA-GM(1,1)-BPNN and GA-GM(1,1)-PSO-BPNN models is shown in Fig. 5.

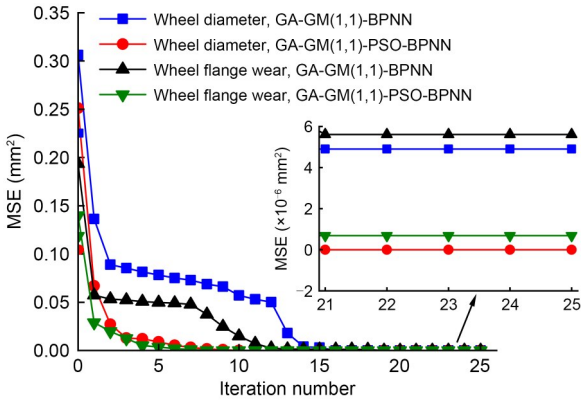

Fig. 5 Error convergence trends of different models

With the optimization ability of the PSO algorithm, the neural network had a relatively faster convergence speed and converged to a lower MSE, which makes predictive results more accurate.

The predictive values of wheel diameter using the traditional GM(1, 1) model and the proposed GA-GM(1,1), GA-GM(1,1)-BPNN, and GA-GM(1,1)-PSO-BPNN models are shown in Fig. 6a. Based on Fig. 6a, the traditional non-equidistant GM(1,1) model reflected the overall changing trend of the measured wear data series, but could not well track the local variation. By correcting the initial predicted residual error series using the BPNN model, the forecasted data were closer to the actual values in each period. The contributions of GA to the traditional GM(1,1) model and PSO algorithm to BPNN model can be clearly observed in Fig. 6a, which indicates that the GA and PSO algorithms can bring a strong approximation ability to GM(1,1) and BPNN models. To choose the best model accurately, the REs between the actual and forecasted data were compared in Fig. 7a and the MRE, MAE, MAPE, and MSE of each model in Table 3. With the aid of the GA, BPNN, and PSO algorithms, all three proposed models, GA-GM(1,1), GA-GM(1,1)-BPNN, and GA-GM(1,1)-PSO-BPNN, had significantly smaller errors than the traditional GM(1,1) model in both the fitting and prediction zones. From highest to lowest, the fitting and prediction performance ranking

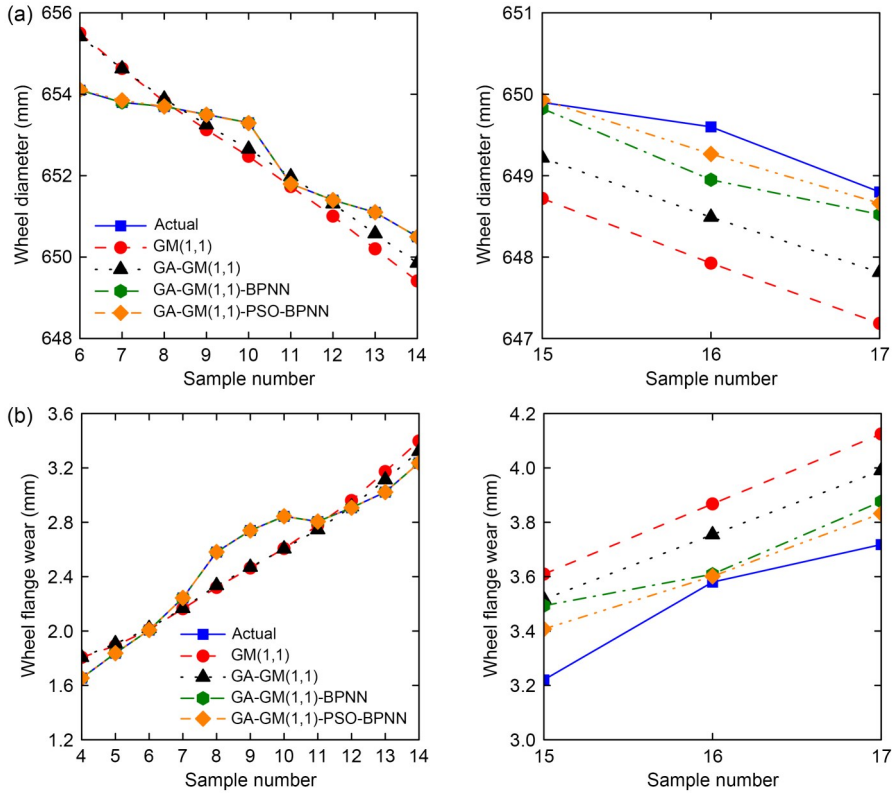

Fig. 6 Actual and predictive data curves using different models of wheel diameter (a) and wheel flange wear (b)

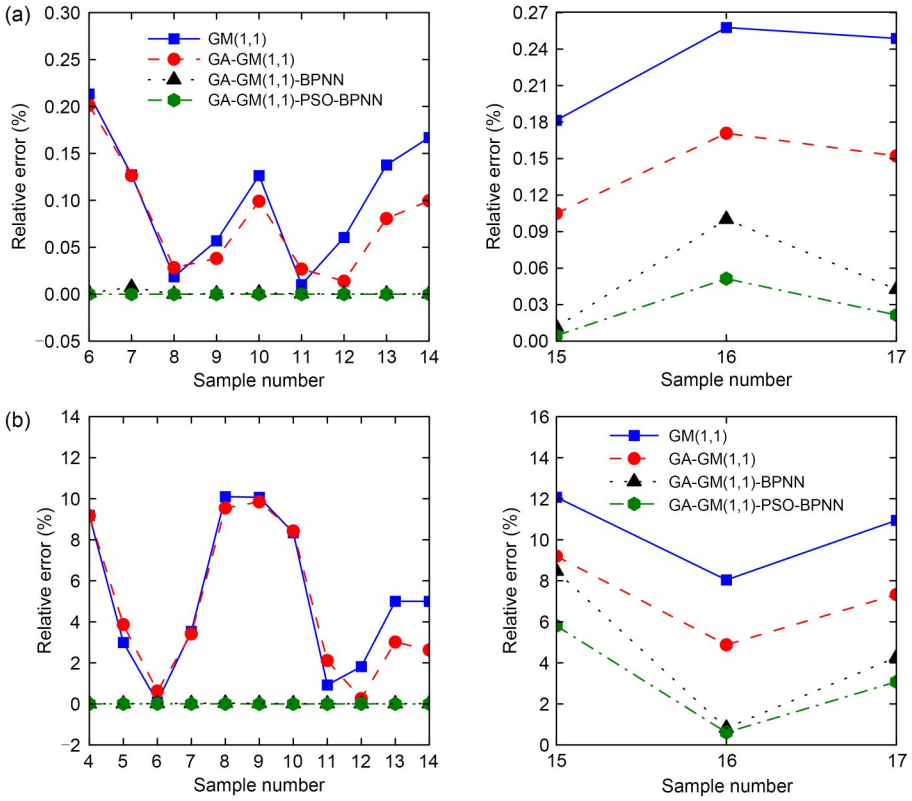

Fig. 7 REs of the predictive data of wheel diameter (a) and wheel flange wear (b)

Table 3 Errors of different models in the fitting zone and prediction zone

Item	Model	Fitting				Prediction			
		MRE (%)	MAE (mm)	MAPE	MSE (mm^2)	MRE (%)	MAE (mm)	MAPE	MSE (mm^2)
Wheel diameter	GM(1,1)	0.213	0.572	9×10^{-4}	0.519	0.258	1.29	0.002	1.756
	GA-GM(1,1)	0.201	0.498	8×10^{-4}	0.424	0.171	0.79	0.002	0.673
	GA-GM(1,1)-BPNN	0.008	0.009	2×10^{-5}	3×10^{-4}	0.102	0.34	6×10^{-4}	0.168
	GA-GM(1,1)-PSO-BPNN	2×10^{-4}	6×10^{-5}	2×10^{-6}	6×10^{-6}	0.051	0.17	3×10^{-4}	0.044
Wheel flange wear	GM(1,1)	10.10	0.132	0.952	0.026	12.07	0.361	0.104	0.133
	GA-GM(1,1)	9.85	0.119	0.048	0.022	9.19	0.248	0.071	0.064
	GA-GM(1,1)-BPNN	0.04	3×10^{-4}	2×10^{-4}	1×10^{-4}	8.47	0.154	0.045	0.033
	GA-GM(1,1)-PSO-BPNN	2×10^{-6}	1×10^{-6}	2×10^{-5}	4×10^{-6}	5.85	0.084	0.023	0.008

of the four methods was GA-GM(1,1)-PSO-BPNN> GA-GM(1,1)-BPNN>GA-GM(1,1)>GM(1,1). Specifically, the GA-GM(1,1)-PSO-BPNN model performed best among the four models based on its lowest MRE, MAE, MAPE, and MSE values of 2×10^{-6}, 6×10^{-5} mm, 2×10^{-6}, and 6×10^{-6} mm^2 in the fitting zone and 0.051%, 0.17 mm, 3×10^{-4}, and 0.044 mm^2 in the prediction zone, respectively. Conversely, the traditional GM(1,1) model came in last with the highest MRE, MAE, MAPE, and MSE values of 0.213%, 0.572 mm, 9×10^{-4}, and 0.519 mm^2 in the fitting zone and 0.258%, 1.29 mm, 0.002, and 1.756 mm^2 in the prediction zone, respectively. Although the improved GA-GM(1,1) model was more accurate than the traditional GM(1,1) model, its overall effect was still not ideal.

The forecasted values of wheel flange wear and the prediction models' errors are shown in Fig. 6b and Fig. 7b, respectively. Similar to wheel diameter, the GA-GM(1,1)-PSO-BPNN model had the highest reliability and validity in fitting and predicting wheel flange wear, followed by the GA-GM(1,1)-BPNN, GA-GM(1,1), and GM(1,1) models. The MRE, MAE,

MAPE, and MSE values of the GA-GM(1,1)-PSO-BPNN model were 2×10^{-8}, 1×10^{-6} mm, 2×10^{-5}, and 4×10^{-6} mm^2 in the fitting zone, and 5.85%, 0.084 mm, 0.023, and 0.008 mm^2 in the prediction zone, respectively, which were much lower than those of the traditional GM(1,1) model with corresponding values of 10.1%, 0.132 mm, 0.952, and 0.026 mm^2 in the fitting zone and 12.07%, 0.361 mm, 0.104, and 0.133 mm^2 in the prediction zone. The errors of the other two models lay between those of the GM(1,1) and GA-GM(1,1)-PSO-BPNN models.

The simulation times of wheel diameter and wheel flange wear prediction using the four models are listed in Table 4. The more complex the model, the longer it took to complete the forecast task. In particular, the GA-GM(1,1)-PSO-BPNN model required a few extra minutes but this was not significant considering its higher efficiency and robustness.

5 Conclusions

By using the non-equidistant GM(1,1) model combined with GA, in this study, we predicted the wheel wear of a light rail train operated on the Changchun Rail Transit Line 4 with respect to running mileage from 894857 to 959875 km according to the field measured wear of mileage from 465523 to 865527 km. The results showed how the GA presented can be used to improve the traditional GM(1,1) model. The initial residual errors of the GA-GM(1, 1) prediction series were corrected by the BPNN model. The optimized weights and biases of the network were automatically searched by a PSO algorithm. The fitting and prediction accuracies of these four models were estimated by MRE, MAE, MAPE, and MSE. The following conclusions were drawn:

1. Due to its ability to search the entire parameter space while skipping local-optimal points, a GA could be introduced to optimize the background value of a grey model. The improved GA-GM(1,1) model lowered both the fitting and prediction errors of the classic GM(1,1) model.

2. Combining the advantages of the improved model GA-GM(1,1) in linear prediction and the neural network model in stochastic data prediction, the GA-GM(1,1)-BPNN model further upgraded the fitting and prediction performances.

3. Benefitting from the contributions of the weight and bias optimized by the PSO algorithm, the GA-GM(1,1)-PSO-BPNN model showed the most reliable performance with the least fitting and forecasting MRE, MAE, MAPE, and MSE values of the four models. The GA-GM(1,1)-PSO-BPNN model fitted the observed data extremely well and its prediction results matched the observed data most closely.

4. The GA-GM(1,1)-PSO-BPNN model is more complex but more efficient. It can accurately track the changing trend of wheel wear, overcoming the impacts of the nonlinear and random characteristics of the measured wear data in the case of small samples. Though this model usually takes more time in application, the extra time is insignificant considering its higher efficiency and robustness.

Acknowledgments

This work is supported by the National Natural Science Foundation of China (No. 52178436) and the Shanghai Collaborative Innovation Research Center for Multi-network & Multi-modal Rail Transit, China.

Author contributions

Xinwen YANG designed the research. Yanyan ZHANG processed the corresponding data and wrote the first draft of the manuscript. Xinwen YANG helped to organize the manuscript. Zhiang SUN, Kaiwen XIANG, and Anguo ZUO revised and edited the final version.

Conflict of interest

Yanyan ZHANG, Xinwen YANG, Zhiang SUN, Kaiwen XIANG, and Anguo ZUO declare that they have no conflict of interest.

References

Cai H, Wang YL, Song CW, et al., 2022. Prediction of surface subsidence based on PSO-BP neural network. *Journal of Physics: Conference Series*, 2400(1):012046. https://doi.org/10.1088/1742-6596/2400/1/012046

Table 4 Prediction times of different models

Item	Time (s)			
	GM(1,1)	GA-GM(1,1)	GA-GM(1,1)-BPNN	GA-GM(1,1)-PSO-BPNN
Wheel diameter	2.81×10^{-3}	0.15	1.72	591.44
Wheel flange wear	3.07×10^{-3}	0.14	1.27	523.01

Cai L, Lin JD, Liao XY, 2022. Life prediction of ship CXF cable using a non-equidistant grey model with small samples. *IEEE Transactions on Power Delivery*, 37(6):5094-5101. https://doi.org/10.1109/TPWRD.2022.3168552

Chang JH, Zhang JZ, Li WG, et al., 2022. Big data dressing recommendation based on ant colony algorithm to optimize BP network. Proceedings of the Second International Conference on Advanced Algorithms and Signal Image Processing (AASIP 2022), article 124751W. https://doi.org/10.1117/12.2659700

Chen ZW, 2019. Research on Wheel Size Prediction and Re-Profiling Strategy for the Wheel-Set of High-Speed EMU. MS Thesis, Southwest Jiaotong University, Chengdu, China (in Chinese). https://doi.org/10.27414/d.cnki.gxnju.2019.002855

Chi ZX, Lin J, Chen RR, et al., 2020. Data-driven approach to study the polygonization of high-speed railway train wheel-sets using field data of China's HSR train. *Measurement*, 149:107022. https://doi.org/10.1016/j.measurement.2019.107022

Chudzikiewicz A, Korzeb J, 2018. Simulation study of wheels wear in low-floor tram with independently rotating wheels. *Archive of Applied Mechanics*, 88(1-2):175-192. https://doi.org/10.1007/s00419-017-1301-6

Correa N, Vadillo EG, Santamaria J, et al., 2016. A versatile method in the space domain to study short-wave rail undulatory wear caused by rail surface defects. *Wear*, 352-353: 196-208. https://doi.org/10.1016/j.wear.2016.02.012

Deng YQ, Liu L, Li MY, et al., 2023. A data-driven wheel wear prediction model for rail train based on LM-OMP-NARXNN. *Journal of Computing and Information Science in Engineering*, 23(2):021012. https://doi.org/10.1115/1.4054488

Fan N, Wang SW, Liu CX, et al., 2017. Wheel wear prediction of high-speed train using NAR and BP neural networks. IEEE International Conference on Internet of Things (iThings) and IEEE Green Computing and Communications (GreenCom) and IEEE Cyber, Physical and Social Computing (CPSCom) and IEEE Smart Data (SmartData), p.126-130. https://doi.org/10.1109/iThings-GreenCom-CPSCom-SmartData.2017.24

Han P, Zhang WH, 2015. A new binary wheel wear prediction model based on statistical method and the demonstration. *Wear*, 324-325:90-99. https://doi.org/10.1016/j.wear.2014.11.022

Huang GB, Zhu QY, Siew CK, 2006. Extreme learning machine: theory and applications. *Neurocomputing*, 70(1-3):489-501. https://doi.org/10.1016/j.neucom.2005.12.126

Jiang YZ, Zhong WS, Wu PB, et al., 2019. Prediction of wheel wear of different types of articulated monorail based on co-simulation of MATLAB and UM software. *Advances in Mechanical Engineering*, 11(6):1-13. https://doi.org/10.1177/1687814019856841

Jiang ZQ, Banjevic D, E MC, et al., 2017. Optimizing the re-profiling policy regarding metropolitan train wheels based on a semi-Markov decision process. *Proceedings of the Institution of Mechanical Engineers, Part O: Journal of Risk and Reliability*, 231(5):495-507. https://doi.org/10.1177/1748006X17710816

Li Y, Tang MA, Gu BH, et al., 2015. Forecast research on trucks wheel tread wear based on grey changeable weight combination model. *Journal of Railway Science and Engineering*, 12(1):160-165 (in Chinese). https://doi.org/10.19713/j.cnki.43-1423/u.2015.01.026

Li Y, Luan YZ, Zhang ST, 2016. Application of the optimization of background value in non-equidistant GM(1,1) model in the settlement prediction. *Beijing Surveying and Mapping*, (5):48-52 (in Chinese). https://doi.org/10.19580/j.cnki.1007-3000.2016.05.010

Liao GL, 2014. Research on the Security State Prediction and Lathing Strategy Optimization for the Wheelset of Urban Rail Train. MS Thesis, Beijing Jiaotong University, Beijing, China (in Chinese). https://doi.org/10.7666/d.Y2602690

Liu BL, Zhang YF, Pan DB, et al., 2024. Amphibious vehicle's resistance optimization through neural networks and genetic algorithms. *Physics of Fluids*, 36(6):065129. https://doi.org/10.1063/5.0210244

Liu F, Yang XW, Chen DW, et al., 2022. Wheel wear characteristics analysis of Changchun 70% low-floor light rail vehicles. *Urban Mass Transit*, 25(9):11-15 (in Chinese). https://doi.org/10.16037/j.1007-869x.2022.09.003

Łuczak B, Firlik B, Staśkiewicz T, et al., 2020. Numerical algorithm for predicting wheel flange wear in trams–validation in a curved track. *Proceedings of the Institution of Mechanical Engineers, Part F: Journal of Rail and Rapid Transit*, 234(10):1156-1169. https://doi.org/10.1177/0954409719882807

Ning Y, Jin YP, Peng YD, et al., 2022. Small obstacle size prediction based on a GA-BP neural network. *Applied Optics*, 61(1):177-187. https://doi.org/10.1364/AO.443535

Pradhan S, Samantaray A, Bhattacharyya R, 2019. Multi-step wear evolution simulation method for the prediction of rail wheel wear and vehicle dynamic performance. *Simulation*, 95(5):441-459. https://doi.org/10.1177/0037549718785023

Shebani A, Iwnicki S, 2018. Prediction of wheel and rail wear under different contact conditions using artificial neural networks. *Wear*, 406-407:173-184. https://doi.org/10.1016/j.wear.2018.01.007

Su KX, Zhang JW, Zhang JW, et al., 2023. Optimisation of current collection quality of high-speed pantograph-catenary system using the combination of artificial neural network and genetic algorithm. *Vehicle System Dynamics*, 61(1): 260-285. https://doi.org/10.1080/00423114.2022.2045029

Wang MQ, Wang Y, Chen EL, et al., 2022a. High-speed train tread wear prediction model based on I-ML-ELM. *Chinese Journal of Theoretical and Applied Mechanics*, 54(6): 1720-1731 (in Chinese). https://doi.org/10.6052/0459-1879-21-692

Wang MQ, Jia SX, Chen EL, et al., 2022b. Research and application of neural network for tread wear prediction and

optimization. *Mechanical Systems and Signal Processing*, 162:108070. https://doi.org/10.1016/j.ymssp.2021.108070

Wang SW, Guo H, Zhang SY, et al., 2022. Analysis and prediction of double-carriage train wheel wear based on SIMPACK and neural networks. *Advances in Mechanical Engineering*, 14(3):1-12. https://doi.org/10.1177/16878132221078491

Wojciechowski Ł, Gapiński B, Firlik B, et al., 2020. Characteristics of tram wheel wear: focus on mechanism identification and surface topography. *Tribology International*, 150:106365. https://doi.org/10.1016/j.triboint.2020.106365

Xing ZY, Mao LL, Liao GL, et al., 2014. Forecasting of wheelset size of urban rail train based on PSO-SVM model. *Journal of Shenyang University of Technology*, 36(4): 411-415 (in Chinese). https://doi.org/10.7688/j.issn.1000-1646.2014.04.10

Xu XP, 2021. Research on Wheelset Parameter Detection Technology and Wear Prediction. MS Thesis, Nanjing University of Science & Technology, Nanjing, China (in Chinese). https://doi.org/10.27241/d.cnki.gnjgu.2021.003383

Yang Z, Xing ZY, Wang L, et al., 2018. Optimization of wheel re-profiling strategy based on statistical wear model. *Railway Standard Design*, 62(1):142-148 (in Chinese). https://doi.org/10.13238/j.issn.1004-2954.201703170006

Yuan K, Xu SA, Fu YQ, et al., 2024. Research on weigh-in-motion algorithm of vehicles based on WOSA-BP. *Chinese Journal of Sensors and Actuators*, 37(1):50-57 (in Chinese). https://doi.org/10.3969/j.issn.1004-1699.2024.01.008

Zhang SR, Wang BT, Li XE, et al., 2016. Research and application of improved gas concentration prediction model based on grey theory and BP neural network in digital mine. *Procedia CIRP*, 56:471-475. https://doi.org/10.1016/j.procir.2016.10.092

Zhang Y, Zhang JW, Luo L, et al., 2019. Optimization of LMBP high-speed railway wheel size prediction algorithm based on improved adaptive differential evolution algorithm. *International Journal of Distributed Sensor Networks*, 15(10):1-9. https://doi.org/10.1177/1550147719881348

Zhong LS, Chen LY, Gong JH, et al., 2015. Prediction of wheel tread wear volume based on least squares support vector machine optimized by coupled simulated annealing. *Application Research of Computers*, 32(2):397-402 (in Chinese). https://doi.org/10.3969/j.issn.1001-3695.2015.02.018

Zhu AH, Yang S, Li Q, et al., 2019. Research on prediction of metro wheel wear based on integrated data-model-driven approach. *IEEE Access*, 7:178153-178166. https://doi.org/10.1109/ACCESS.2019.2950391

Zhu Y, Wang WJ, Lewis R, et al., 2019. A review on wear between railway wheels and rails under environmental conditions. *Journal of Tribology*, 141(12):120801. https://doi.org/10.1115/1.4044464